CIMAC CONGRESS 25
ZURICH, MAY 19 – 23, 2025

2025 | 362

A pathway to develop a methanol combustion concept for retrofit propulsion applications

Retrofit Solutions

Maximilian Malin, LEC GmbH

Nicole Wermuth, Institute of Thermodynamics and Sustainable Propulsion Systems, Graz University of Technology, Austria
Marcel Lackner, LEC GmbH
Claudia Schubert-Zallinger, Institute of Thermodynamics and Sustainable Propulsion Systems, Graz University of Technology, Austria
Anton Tilz, LEC GmbH
Michael Engelmayer, LEC GmbH
Adam Klingbeil, Wabtec Corporation
Thomas Kammerdiener, AVL List GmbH
Martin Bernhaupt, Robert Bosch AG

ABSTRACT

To achieve a significant reduction in greenhouse gas emissions in the transportation sectors, such as rail and maritime applications, the use of renewable fuels is a crucial element. Due to the long service life of large-bore engines in the transport sector, retrofit solutions of existing engine platforms must be considered in order to reach this target in the near future. Among the renewable fuels, methanol is particularly well-suited for retrofit solutions, as it is easier to handle in terms of fuel storage, global availability, safety requirements, and emissions compared to other sustainable fuels such as ammonia or hydrogen. Given that today a significant number of engines in the transport sector are diesel engines and redundancy requirements need to be considered a diesel-methanol dual-fuel concept represents an attractive option for retrofit solutions.

The objective of this paper is to describe a pathway for the development of a port fuel injection (PFI) dieselmethanol dual-fuel combustion concept for retrofit applications. A multi-stage approach was employed to investigate the combustion concept in several steps. This approach established a strong link between fundamental methanol spray investigation and singe cylinder engine (SCE) testing. In a first step methanol spray investigations for medium range rail pressures were performed in an optically accessible spray chamber for various injector configurations. The results of the optical investigation served as input for the calibration of the spray sub-models of a 3D-CFD simulation of the spray chamber. The calibrated 3D-CFD simulation was used to investigate and optimize the methanol-air mixture formation in the intake system of the engine. The starting point for the development of the methanol combustion process was a state-of-the-art diesel engine with a diesel common rail injection system. The methanol injector was integrated close to the intake port, but was not part of the cylinder head, which allowed the use of the standard cylinder head without modification, providing an easy retrofit solution (low complexity). The diesel-methanol dual-fuel combustion concept was tested on the SCE, with particular focus on the evaluation of combustion performance, methanol substitution rates and exhaust emissions. The paper concludes with an assessment of the limitations of the PFI methanol combustion concept.

1 INTRODUCTION

In November 2024 the Copernicus Climate Change Service reported that 2024 was on track to become the warmest year on record and the first year with an annual temperature more than 1.5 °C above the pre-industrial level [1]. This highlights the urgency for all industrial sectors to reduce their emissions of greenhouse gases (GHG). Medium speed internal combustion engines that are employed in propulsion applications such as locomotives or shipping vessels are no exceptions.

In the US where – according to the Environmental Protection Agency – rail contributes approximately 2 % to the annual GHG emissions from transportation [2], the Federal Railroad Administration (FRA) launched the "Climate and Sustainability Program" that coordinates activities and initiatives that improve air quality and reduce GHG emissions. Shifting the operation of locomotives from traditional energy to sustainable fuel sources is one of the key FRA research initiatives [3]. Some railroads are already increasing the share of low-carbon fuels such as biodiesel or renewable diesel in their operations [4]. Also, in Brazil railroad operators are exploring a number of alternative fuels including biodiesel, hydrotreated vegetable oil, ethanol, and ammonia [5]. While battery-electric and fuel cell propulsion systems are also under investigation, retrofitting an existing freight locomotive for operation with a new fuel is often considered more cost-effective [6].

In order to reduce GHG emissions from the shipping sector the EU's Emissions Trading System has been extended since 2024 to cover carbon dioxide (CO_2) emissions from all large ships entering EU ports [7] and in January 2025 the FuelEU Maritime Regulation came into effect and promotes the use of renewable, low-carbon fuels and clean energy technologies for ships by setting maximum limits for the GHG intensity of the energy used on board [8]. The United States Government developed an "Action plan for maritime energy and emissions innovation" with the transition to a new set of low-GHG fuels for ocean-going vessels, the use of sustainable drop-in fuels where necessary and the adoption of electrification and fuel cell technology for smaller vessels where feasible at its core [9].

In 2024 newbuilds equipped with alternative fuel-capable engine technology were ordered in record numbers. According to DNV's Alternative Fuels Insights platform more than 300 vessels for ammonia and methanol are currently on the orderbooks [10]. Considering the size of the world's merchant fleet of more than 100.000 vessels and the long working life of vessels many ships originally designed to be powered by fossil fuels are likely to remain in service through 2050. Retrofitting these vessels to use carbon-neutral or zero-carbon fuels is going to be a crucial element in the maritime energy transition.

Due to the availability of bunkering options in ports all over the world it is likely that many vessels will have to maintain their ability to run on diesel fuel or marine gas oil as well, thus favoring dual fuel engines. Methanol is one of the top five chemical commodities shipped around the world. It is liquid at ambient temperatures and does not require refrigeration or pressurization for storage and therefore necessitates fewer modifications on board than hydrogen or liquefied natural gas, making it suitable also for smaller vessels with space limitations.

The world's first methanol engine retrofit project on the Stena Germanica took place in 2015 [11] and was followed by several other vessels since. In the meantime, interim guidelines for the safety of ships using methyl / ethyl alcohol as fuel were developed [12] while similar guidelines for ammonia or hydrogen are still outstanding.

Methanol-diesel dual fuel combustion concepts can use high-pressure direct injection of methanol in a mixing controlled combustion process or low-pressure (port-) injection of methanol for a homogenous flame-propagation based combustion process. A high-pressure fuel injection concept has the advantage that no or fewer compromises are required for methanol and diesel back-up operation [13]. Port fuel injection, on the other hand, enables the complete system including injector, fuel pump and piping to be physically small and therefore cost-effective. Port fuel injection systems can be more easily integrated onto the engine and do not require a redesign of the cylinder had so they offer benefits for retrofit applications.

One of the major challenges with port fuel injection designs is maximizing the achievable methanol substitution rate. In [14] it was found that the maximum methanol substitution for a port fuel injection concept was strongly dependent on the charge air temperature with low substitution rates of 45 – 50 % for 35 °C charge air temperature and approximately 20 percentage points higher substitution rates with 65 °C charge air temperature. A strong load-dependance of the substitution rate was reported in [15]. For an engine without variable valve timing capability pressure gradients and misfiring were the limiting factors and substitution rates between 20 and 40 % were achievable. In a different engine with additional variabilities significantly higher substitution rates were achievable, particularly at part load operation.

Still, at full load operation the substitution rate was limited to 50%.

The fuel injection and mixture formation are the critical elements in all of the reported port fuel injection concepts. On one hand an injector position far upstream of the cylinder head benefits from a longer residence time for the fuel evaporation. But on the other hand, the risk of wall wetting also increases depending on droplet size, geometry of the intake manifold and the wall surface temperatures. In [20] the impact of droplet sizes on their ability to follow the air flow in a pipe was investigated and it was found that only droplets smaller than 15 µm could avoid wall impingement, highlighting the need to properly match the engine geometry and the fuel injection arrangement.

This article describes the development process of a retrofit low-pressure methanol port fuel injection dual fuel combustion concept for a serial production medium-speed locomotive application.

2 PATHWAY TO DEVELOP A METHANOL COMBUSTION CONCEPT

The development followed a multi-step approach combining methanol spray characterization, 1D multi-cylinder engine performance simulation, 3D-CFD simulation and finally experimental assessment on a single cylinder research engine (SCE) (Figure *1*). The premise for the concept development was to maintain the production power unit components, in particular the intake manifold, cylinder head and piston assembly as well as the diesel injector of the original Wabtec diesel engine. In dual fuel operating mode, a percentage of diesel is substituted by methanol, while the diesel injection still initiates the combustion process. The engine also retains its full diesel performance capability.

In a first step, a 1D performance simulation model was developed for the 12-cylinder locomotive engine. The simulation model reflects the geometry and dimensioning of the production engine, including intake and exhaust manifold, flow coefficients and turbocharging. For the methanol-diesel operation the model was amended with methanol port fuel admission valves and additional actuators to allow the control of the excess air ratio. The flow rate of the fuel admission valves was used as an input parameter to represent the AFI-LP port fuel injectors that the Robert Bosch AG provided for the experimental investigations. The injection duration was adjusted to achieve the desired load and engine speed. A normalized heat release rate (HRR) curve was used in lieu of a combustion model for each of the 8 notches in the locomotive notch schedule. Simulations were performed for various methanol substitution rates with a focus on required methanol injection quantities, methanol injection timing and duration, achievable excess air ratios, boost pressure and exhaust gas pressure as well as their combined impact on the maximum cylinder pressure. These simulation results can serve as a guideline for the boundary conditions for the investigation on the SCE.

Based on the initial concept layout, the methanol fuel injection system was designed for low to medium injection pressures up to 50 bar. Different spray forming caps with varying numbers of spray hole configurations were designed and manufactured by Bosch for the experimental investigations. The test matrix included different numbers of spray holes, different flow rates and different spray hole geometries. For an assessment of the impact of the spray hole diameter spray forming caps with a different number of spray holes but same nominal flow rates (i.e., different spray hole diameters) were produced and tested on an injector test rig at Bosch. The rate of injection (ROI) was measured with a HDA injection rate analyzer [21].

In the next stage of the development the methanol spray characterization was conducted in a constant volume spray chamber. Spray investigations with single-hole spray forming caps were performed to assess the influence of spray hole diameter, spray hole length and spray edge rounding on the methanol spray. Multi-hole spray forming caps, designed for the use on the engine, were used to investigate the spray pattern, spray penetration and spray angle.

The results obtained from the spray characterization were utilized for the calibration of the spray sub-models of the 3D-CFD simulation. Therefore, the constant volume spray chamber was modelled in a CFD simulation environment, and spray simulations were conducted with single-hole and multi-hole spray forming caps, with the same boundary conditions as in the experiment. After the calibration process of the spray sub-models, a 3D-CFD engine simulation model was built to investigate the spray development, evaporation, mixture formation, spray-wall interaction and the wall wetting process in the intake ports. In addition to the investigation of the processes in the intake ports, the mixture formation in the combustion chamber from intake valve opening to the start of the diesel injection was investigated. The 3D-CFD engine simulation model could also be used to further optimize the geometry of the spray forming caps, including the number of spray holes, the diameter of the spray holes, and the orientation of each individual spray hole. For significant changes to the geometry of the spray forming cap an

iteration loop with additional tests in the spray chamber and calibration of the spray sub-models might be useful.

The newly developed fuel system and port fuel injectors were integrated on the single-cylinder engine test bed and used in experimental investigations with varying methanol substitution rates. The performance and emissions were evaluated for different load conditions and different operating parameters. In the final stage, the experimental results from the SCE and the results from the 3D-CFD simulation were evaluated and utilized to refine the boundary conditions for the 1D performance simulation of the 12-cylinder engine. In the next steps the refinements might include the heat release rates, knock margins or methanol substitution rate limits. The development loop can be repeated to further improve the combustion concept if necessary.

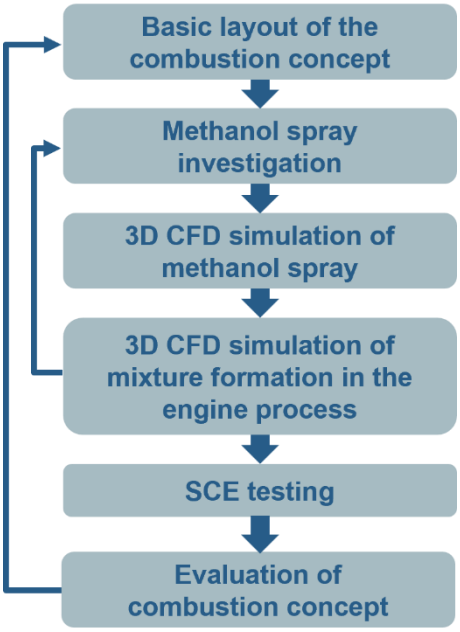

Figure 1. Development pathway for the methanol port fuel injection concept

3 METHANOL SPRAY CHARACTERIZATION

The optical investigation of the liquid and vapor spray of the methanol injector were carried out on a constant volume spray chamber with a total volume of 26 dm^3. For the investigation of the liquid spray, the diffused back illumination (DBI) was employed (cf. [22]), while for the vapor spray, the schlieren technique (cf. [23]) was used. The imaging process was conducted using a Photron SAX-2 high-speed camera, operating at a frame rate of 20,000 frames per second. To ensure statistical validity, each operating point was repeated 20 times. A schematic overview of the experimental setup can be found in Figure *2*.

Four different spray forming caps were investigated in the spray chamber. In Table *1* the specifications of the spray forming caps and the test boundary conditions are listed. For the single hole spray forming caps the impact of the methanol rail pressures and the ratio between spray hole length and spray hole diameter (L/D) were investigated. For the multi hole spray forming cap the investigation focused on the spray pattern.

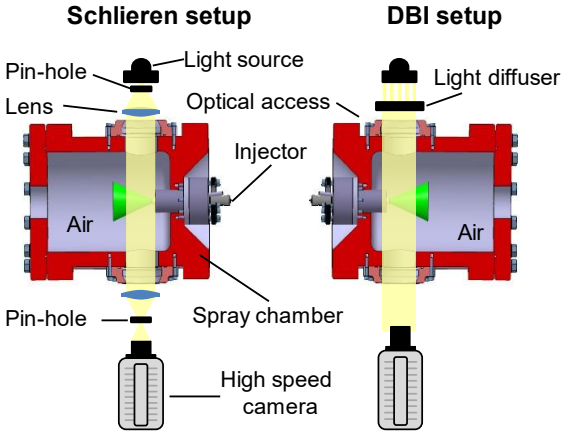

Figure 2. Experimental setup of the spray chamber

For the experiments the spray chamber was filled with air at a pressure of 1 bar[1] and a gas temperature of 50 °C to represent the injection conditions in the engine intake port. The methanol temperature was set to approximately 25 °C. Two distinct methanol injection pressure levels were examined: 50 bar and 10 bar. For all experiments, a constant duration for the injector current (DoC) of 3 ms was selected, irrespective of the boundary conditions.

[1] In this article, all pressure values relating to fuel injection are given in the form of gauge pressure values.

Table 1. Spray forming cap matrix and test conditions

Spray forming cap	Hole number	Hole diameter	Flow rate	L/D	Rail pressure	Chamber pressure
#	-	mm	cm3/30s	-	bar	bar
1	1	0.45	675	1	10 50	1
2	1	0.45	675	2	50	1
3	10	0.56	10350	1	50	1
4	27	0.34	~10350	1	50	1

3.1 Spray image processing

The liquid penetration length, denoted in this paper as spray length, was determined based on a method proposed by Pickett [25]. In this method, experimental optical extinction data created with DBI imaging is processed and converted into the projected liquid volume for which a fixed threshold is used to define the spray length. The projected liquid volume can be compared to CFD data using the same metric [32]. The spray cone angle was defined based on the projected spray area and the spray length as described in [33]. The vapor penetration length and the cone angle of the vapor phase were processed from the schlieren images, and the spray edge was defined by a constant intensity threshold. Based on the spray edge, the penetration length and spray cone angle were calculated [24].

For a qualitative representation of the different methanol sprays in this paper, the raw images of the high-speed camera were used.

3.2 Spray characterization results

A comparison of the liquid and vapor spray development for spray forming cap #1 with a methanol injection pressure of 50 bar is shown in Figure 3.

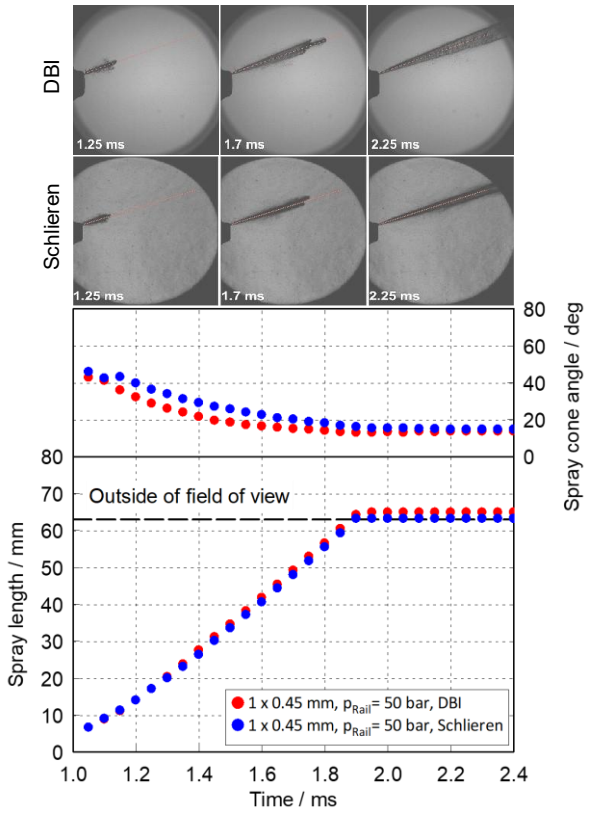

Figure 3. Comparison of DBI and schlieren images and impact on calculated spray metrics for spray forming cap #1

At the start of the injection at approximately 1 ms, both penetration lengths begin to increase with a similar rate until the limit of the optical field of view is reached, which occurs at a distance of approximately 62 mm from the injector tip. The difference in the penetration lengths is small, indicating a low methanol evaporation rate. This is also reflected in the calculated liquid and vapor spray cone angles, which only display small differences at the beginning of the injection process and in the raw images in the upper part of Figure 3 that show a high degree of similarity.

The low evaporation rate of methanol is attributable to the high heat of vaporization of methanol which is more than seven times higher than that of other liquid fuels typically used for port fuel injection, such as gasoline [31]. Consequently, the methanol spray is predominantly composed of liquid droplets, increasing the risk of wall wetting in the intake port.

Due to the small differences between liquid and vapor sprays the following analysis will show only the liquid spray results.

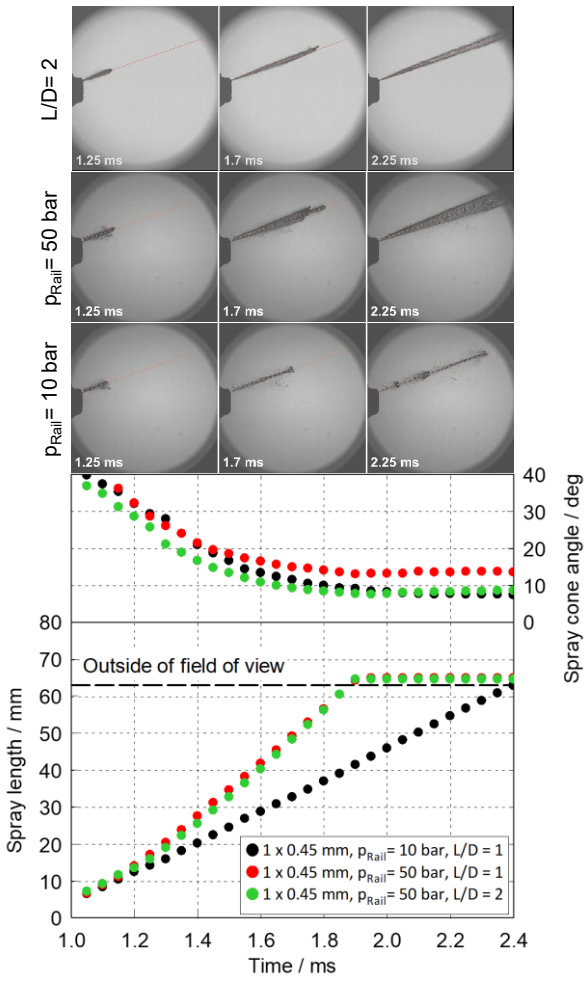

Figure 4. Liquid spray development for spray forming cap #1 and #2 for different methanol injection pressures

The impact of the L/D ratio and a methanol rail pressure increase from 10 to 50 bar on the spray development is illustrated in Figure 4 for spray forming cap #1 (black and red) and #2 (green). As expected, the liquid penetration length exhibits a faster increase for the higher rail pressure, due to higher flow velocity and associated increased momentum flow rate. In addition, the higher rail pressure has been observed to increase the spray cone angle due to the higher flow velocity, which leads to increased eddy-flow structures within the spray hole that intensify the spray break-up [26] . A larger spray cone angle leads to enhanced air entrainment into the spray, thereby promoting favorable conditions for mixture formation [27]. Additionally, it can be assumed that an elevated rail pressure results in a reduction of droplet size in the methanol spray, which is also beneficial for mixture formation [28]. The observed impact of the rail pressure can be further examined in the raw image series presented in the upper part of Figure 4. For all time steps the 10-bar rail pressure case exhibits a shorter penetration length and a narrower spray cone angle than the 50-bar rail pressure case.

The impact of the L/D ratio can be observed by comparing the spray forming caps with a L/D = 1 (red) and L/D = 2 (green) at a constant rail pressure of 50 bar in Figure 4. While the liquid penetration length for both cases is similar, the case with the higher L/D ratio shows a narrower spray cone angle similar to the spray forming cap with unity L/D ratio at the lower rail pressure of 10 bar. This phenomenon has also been observed by [29].

Based on the above findings two multi-hole spray forming caps with 10 holes (#3) and 27 holes (#4) were selected for further investigations for 50 bar rail pressure. As illustrated in the raw DBI images in Figure 5 it is difficult to distinguish each individual spray jet for the 27-hole spray forming cap, indicating that the spray jets begin to merge and spray collapse begins. This is not the case with the 10-hole spray forming cap, where each individual spray jet can be distinguished near the outlet of the spray hole. A collapsing spray pattern increases the liquid penetration length, reduces the spray cone angle, and results in unfavorable conditions for mixture formation [30]. Therefore, the benefit of the smaller hole diameters and the smaller droplets that are expected to improve the mixture formation for the higher hole number spray forming cap is diminished by the collapsing spray.

For all investigated spray forming caps and operating conditions the injector showed low shot-to-shot variability. Taking all the findings from the spray characterization into account the 10-hole nozzle was deemed well-suited for the given application and selected for the 3D-CFD simulation and (among others) for the experimental investigation on the SCE.

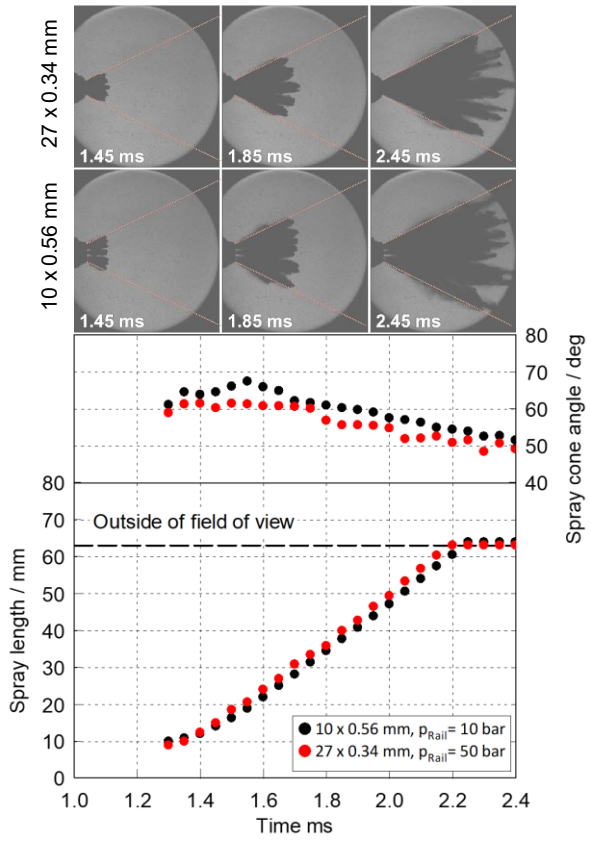

Figure 5. Multi-hole spray forming cap investigation

4 SIMULATION OF METHANOL SPRAY AND MIXTURE FORMATION

3D-CFD simulations of single injection events were carried out to calibrate the simulation models relevant for the injection process with measured liquid spray lengths in the spray chamber. After that, in order to gain a deeper understanding of the mixture formation process in the intake manifold of the locomotive engine, 3D-CFD simulations of one SCE operating point were performed. The software employed for all simulations was AVL FIRE™ from AVL List GmbH.

4.1 CFD spray modeling and validation

The spray simulation is based on the Discrete Droplet Method (DDM), wherein differential equations for trajectory, momentum, heat and mass transfer are solved and the spray droplets are tracked in the computational domain by means of a Lagrangian approach [16]. The domain itself consisted of the spray chamber presented in Section 3. While the global cell size of the polyhedral mesh was set to 5.3 mm, it was refined and set to 0.5 mm in the vicinity of the spray cone. As this cell size was already considered rather small with regards to application to the engine mesh, cell sizes smaller than 0.5 mm were not investigated. Turbulence was modelled with a Reynolds-averaged Navier-Stokes (RANS) approach using the k-ζ-f model. The injection process was modelled by specifying the injected mass and the normalized ROI of the multi-hole spray forming cap, which was modified to account for the injected mass from a single spray hole. All droplets entering the domain were assigned a constant droplet size diameter of 300 µm based on [17] and a crank-angle dependent spray cone angle. Droplet breakup, drag and evaporation were modelled using the Wave, the Schuller Naumann and the Abramzon Sirignano models, respectively. As no wall film was expected in the spray chamber, no wall film-related models were activated.

In order to enable a comparison of the simulated spray length with experimental data, the simulated liquid volume fraction was converted into projected liquid volume based on the method proposed by Pickett and already briefly described in Section 3. The spray cone angle was calculated the same way as in the experiment (see Section 3.1). The comparison of experimental and simulated liquid spray length and cone angle is presented in Figure *6*. As can be seen, the spray lengths match satisfactorily and only minor differences exist after around 1.4 ms. In contrast, the spray angles deviate from each other until approximately 1.4 ms but agree afterwards.

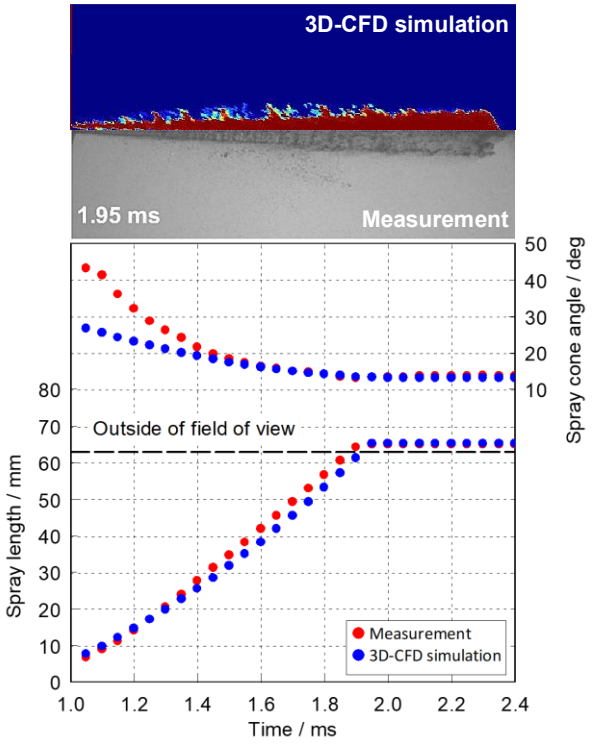

Figure 6. Comparison of measured and simulated spray length and spray cone angle

4.2 Assessment of spray and mixture formation

The simulation setup presented above was also used for the engine cycle simulation, however, some parameters were adapted. First, the cell size in the vicinity of the spray cone was increased to 1 mm due to the overall increased number of cells of the engine mesh compared to the mesh of the spray chamber and the limited computational power. Second, to account for the buildup of a wall film due to spray droplets hitting the intake manifold walls, the wall film model and its sub-models were activated. For instance, entrainment of wall film back into the gas flow in the form of droplets due to shear force is considered by the Schadel-Hanratty model. The droplet size itself is calculated based on the Kataoka Droplet correlation. Third, the sizes of the injected droplets were defined based on a Rosin-Rammler distribution such that the Sauter mean diameter (SMD) calculated with the relation of Hiroyasu [18] is obtained:

$$SMD_1 = 4.12 \cdot Re^{0.12} \cdot We^{-0.75} \cdot \left(\frac{\mu_l}{\mu_a}\right)^{0.54} \cdot \left(\frac{\rho_l}{\rho_a}\right)^{0.18}, \quad (1)$$

$$SMD_2 = 0.38 \cdot Re^{0.25} \cdot We^{-0.32} \cdot \left(\frac{\mu_l}{\mu_a}\right)^{0.37} \cdot \left(\frac{\rho_l}{\rho_a}\right)^{-0.48}, \quad (2)$$

$$SMD = \max(SMD_1, SMD_2). \quad (3)$$

In equations (1) to (3), Re and We stand for Reynolds and Weber number, respectively, μ_l and μ_a are liquid and ambient dynamic viscosity, ρ_l and ρ_a represent liquid and ambient density and the term $\max(...)$ denotes the maximum of the two SMD values.

The polyhedral mesh used for the engine simulation consisted of the intake runner, in which the fuel injector was mounted, the intake and exhaust ports, and the combustion chamber. The global cell size of 8 mm was set based on extensive simulation experience with this engine type; a smaller global cell size was not considered due to the already high computational cost of the spray simulation with its refined area in the vicinity of the spray cone and the rather small time steps during the injection process, both leading to rather long simulation times. In Figure *7*, wall film, spray and vapor masses in the entire intake manifold and the cylinder are depicted for simulations with a constant droplet diameter of 300 µm and Rosin-Rammler distributed droplet sizes with a SMD of around 21 µm. The smaller droplets result in less wall film, presumably because a greater number of droplets follow the flow better and do not hit the wall. This results in more spray mass being present in the intake manifold which again leads to more fuel vapor due to evaporation and subsequently more vaporized fuel in the cylinder. However, the still rather large fuel mass being deposited in the wall film results in relatively little fuel being transported into the cylinder in the current engine cycle. This is why in a next step four consecutive cycles were simulated to capture the wall film buildup in the intake manifold and its impact on fuel transport into the cylinder.

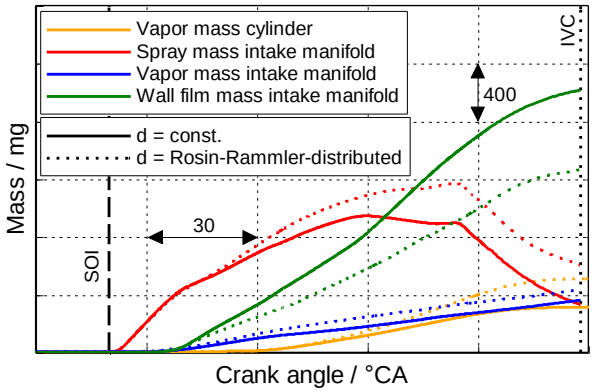

Figure 7. Simulated wall film, spray and vapor masses

Figure *8* again depicts wall film, spray and vapor masses for the aforementioned four consecutive cycles. Like in Figure *7*, in the first cycle the wall film buildup results in relatively little fuel being transported into the combustion chamber. In contrast, the following cycles show a fuel vapor mass in the cylinder at intake valve closing (IVC) that is approximately 5 times higher compared to the first cycle. This is mainly due to evaporation of the wall film and the trapped spray droplets in the intake manifold in the period between IVC of the previous cycle and intake valve opening (IVO) of the current cycle. As soon as the intake stroke starts, the fuel vapor accumulated in the intake port is carried into the cylinder along with the injected fuel spray that does not hit any wall. Since the focus of the simulation was on the wall film buildup in the intake port, the cylinder domain was deactivated at IVC which is why the trace of the vapor mass in the cylinder ends at each IVC. Detailed validation of the wall film model and its parameters will be the subject of future research.

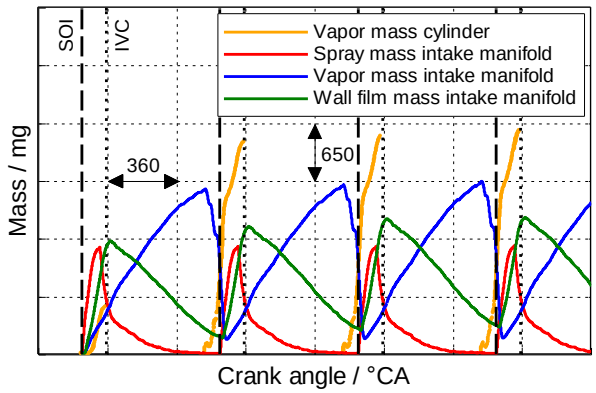

Figure 8. Simulated wall film, spray and vapor masses of the multi-cycle simulation

The mixing of fuel vapor and air already in the intake port as well as the early inflow of this mixture into the cylinder and the resulting long time that is available for further mixing until injection of the pilot fuel results in high in-cylinder mixture homogeneity. The latter was quantified by the uniformity index (UI) of the equivalence ratio ϕ, given by [19]

$$UI = 1 - \frac{1}{2} \cdot \frac{\sum_{i=1}^{N} \left(\frac{|\phi_i|}{\bar{\phi}} - 1 \right) \cdot V_i}{\sum_{i=1}^{N} V_i}, \qquad (4)$$

where the mean equivalence ratio is calculated as follows:

$$\bar{\phi} = \frac{\sum_{i=1}^{N} |\phi_i| \cdot V_i}{\sum_{i=1}^{N} V_i}. \qquad (5)$$

In equations (4) and (5), N is the total number of cells of the computational domain and V_i is the volume of the i-th cell. The UI trace of the in-cylinder mixture of the fourth cycle is depicted in Figure *9*. In addition, cuts through part of the intake port and the cylinder are shown and referred to in brackets in the following paragraph. As the relatively small cylinder volume close to top dead center (TDC) is quickly occupied by fuel-air mixture after IVO (see cuts at IVO + 10 °CA and SOI), the UI increases rapidly, while it decreases after start of injection (SOI) because of the aspiration of mostly pure air and only little methanol spray (see cut at SOI + 15 °CA) which leads to a kind of "de-mixing" and dilution of the in-cylinder mixture. After IVC, mixing progresses and the mentioned high in-cylinder mixture homogeneity is reflected in UI values greater than 0.99, with unity being the maximum possible value, at the start of the diesel injection (see cut at SOI Diesel). In addition, fuel mixture retained in the intake port just upstream of the intake valves can be seen which is scavenged into the exhaust port during the valve overlap phase.

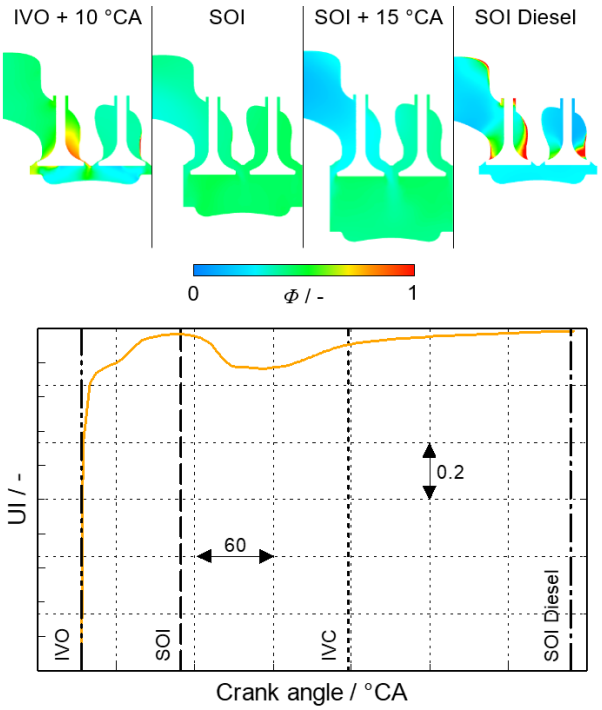

Figure 9. Uniformity index trace of the in-cylinder mixture and cuts through part of the intake port and the cylinder indicating ϕ

5 METHANOL ENGINE COMBUSTION ASSESSMENT

The favorable injector and spray forming cap configurations from the spray characterization and the 3D-CFD simulation were carried over for the assessment of the diesel-methanol combustion concept on the SCE. The diesel power unit, including cylinder head, piston, piston ring pack, and connecting rod, was carried over from the serial production engine. Only small modifications were made to integrate the methanol injector close to the intake port. With this engine configuration the impact of the energetic diesel fraction and the excess air ratio (EAR) on the combustion performance and exhaust gas emissions was investigated.

5.1 Experimental test set-up

The engine investigations were carried out on a medium-speed 4-stroke single cylinder research engine (SCE) with a displacement volume of 15.7 liters. The engine can be equipped with different pistons allowing the adjustment of the compression ratio and combustion chamber geometry. For the investigation of the diesel-methanol operation the series diesel piston crown with a non-reentrant piston bowl and a compression ratio of 17:1 was used. The diesel injector was centrally located and

was capable of operating at full diesel load, as well as providing pilot diesel for diesel-methanol operation. The methanol injector was integrated near the intake port, but was not a part of the cylinder head, allowing the use of the series cylinder head without modification. The low-swirl cylinder head was equipped with two intake and two exhaust valves. Exchanging the cam shaft lobes allows a modification of the valve lift curves. Additionally, the valve timing can be adjusted individually for the intake and the exhaust valves. For this investigation an intake valve lift profile with intake valve closing at bottom dead center was selected. The engine configuration is summarized in Table 2.

Table 2: SCE configuration

General information	
Rated speed	995 min^{-1}
Displacement	15.7 dm^3
Bore	250 mm
Valve timing	Typical diesel valve timing
Number of intake and exhaust valves	2/2
Charge air	Provided by external compressors with up to 10 bar boost pressure
Balance of inertia forces	2 balancing shafts to compensate for first order inertia forces
Diesel injector	Bosch common rail injector
Methanol injector	Bosch AFI-LP
Spray forming cap	Different multi-hole spray forming caps

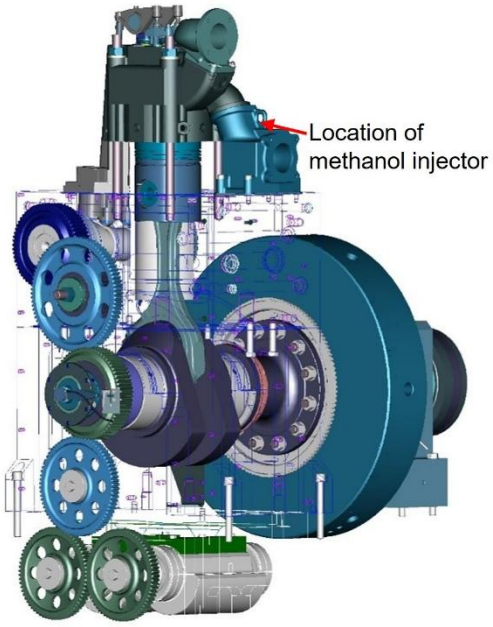

Figure 10. SCE with mass balance system

All engine fluids including cooling water, lubricating oil, and charge air were controlled to ensure well-defined and reproducible testing conditions. Instead of a turbocharger, an air compressor upstream of the engine and a flap in the engine exhaust system were used to adjust intake and exhaust manifold pressures. A flush mounted piezoelectric cylinder pressure transducer enabled real-time calculation of the indicated mean effective pressure of each cycle. Figure 10 shows a schematic figure of the SCE with the position of the methanol injector.

In this article, a distinction is made between two different EARs. The global EAR (EAR_{gl}) is taking the masses of methanol and diesel into account (Equation 6), whereas the methanol EAR (EAR_{meth}) considers only the methanol mass and therefore describes the background mixture in the combustion chamber before the start of diesel injection (Equation 7).

$$EAR_{gl} = \frac{m_{air}}{m_{meth} * AFR_{meth} + m_{diesel} * AFR_{diesel}} \quad (6)$$

$$EAR_{meth} = \frac{m_{air}}{m_{meth} * AFR_{meth}} \quad (7)$$

The following section presents results from the engine operation with a constant mean effective pressure (IMEP) of 23.7 bar and engine speed of 995 rpm representative of Notch 8 of the MCE. Starting from the baseline diesel operating point, the energetic diesel fraction (φ_{Diesel}, defined as diesel energy divided by total fuel energy supplied to the engine) was incrementally reduced and the methanol mass flow rate was increased by increasing the injection duration of the methanol injector. All other engine operating settings such as methanol rail pressure, diesel rail pressure, methanol injection timing, EAR, intake temperature, exhaust backpressure and combustion phasing (MFB50%) were held constant. The latter was achieved by adjusting the start of injection (SOI) of the diesel injector. The diesel fraction reduction was continued until either the cyclic variability, represented by the coefficient of variation of the IMEP (CoV_{IMEP}), exceeded a predefined threshold value or combustion anomalies such as misfire or pre-ignition occurred. The variation of the energetic diesel fraction was performed for different EAR_{gl} in a range from 1.6 to 2.3.

5.2 Experimental results

The achievable methanol-diesel operating range as well as a diesel operating point is shown in Figure 11 together with the brake specific methanol emissions (BSMeOH) and the brake specific NOx emissions (BSNOx).

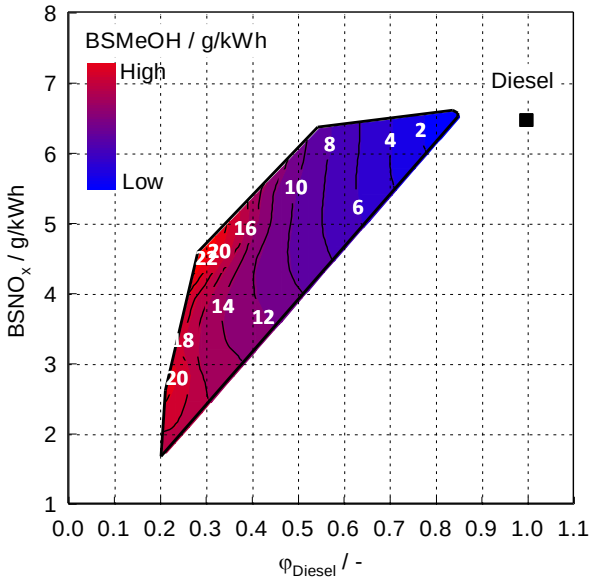

Figure 11. Methanol emissions in the methanol-diesel operating window

Diesel energetic fractions as low as 0.2 could be achieved. Reducing the energetic diesel fraction led to a reduction of the NOx emissions due to a shift from mixing-controlled combustion to premixed combustion and lower process temperatures as a consequence of methanol evaporation. With the lowest energetic diesel fraction, NOx emissions below 2 g/kWh could be achieved. The methanol emissions showed the opposite trend, with higher values for lower diesel fractions and are expected to be impacted by in-cylinder processes and gas exchange (cf. Figure 9). At high diesel fractions, the lean methanol/air mixture is consumed by the dominant diesel jets and the proportion of premixed flame propagation in the combustion chamber is low. In addition, the methanol concentration of the mixture that is trapped in crevices and escapes combustion is rather low. For lower diesel fractions the reliance on flame propagation increases and effects such as wall quenching become more relevant. The scavenging losses that occur during gas exchange with a high valve overlap also increase with higher methanol fraction.

The brake specific carbon monoxide emissions (BSCO) that show values below 1 g/kWh for diesel operation increase significantly for methanol-diesel operation, even with small fractions of methanol, as illustrated in Figure 12. A differentiation of carbon monoxide from diesel combustion on one hand and premixed methanol combustion on the other hand was not feasible with the available exhaust gas analysis, but given the significant difference in CO emissions between diesel and dual fuel operation, it is likely that the majority of the CO emissions are coming from incomplete methanol combustion. Potential impact factors are the reduced gas temperature due to methanol evaporation and lower oxygen fractions in the methanol-air mixture as well as incomplete combustion of methanol due to low flame speed and flame quenching.

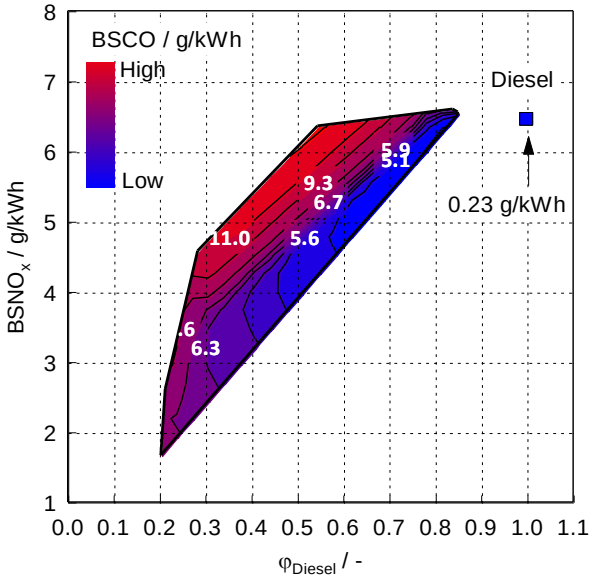

Figure 12. Carbon monoxide emissions in the methanol-diesel operating window

The highest BSCO values occur for intermediate diesel fractions. At low diesel fractions, the EAR_{meth} is lower and the flame temperature and flame speed in the premixed methanol-air mixtures can better support complete combustion. At high diesel fractions, EAR_{meth} is higher resulting in potentially slower flame propagation, but the significant diesel combustion energy provides an energy source to consume the incomplete products of the lean methanol combustion.

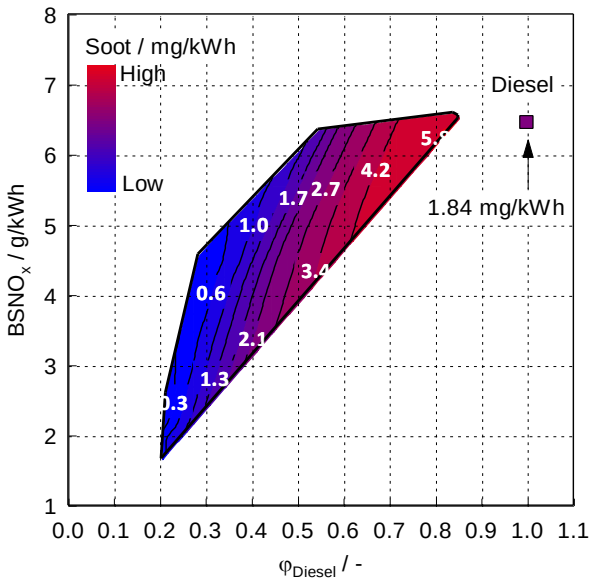

Figure 13. Soot emissions in the methanol-diesel operating window

Figure 13 shows the measured soot emissions with a strong increase from pure diesel operation to a diesel fraction of 0.8 and a continuous decrease with further diesel fraction reduction. With high diesel fractions, it is thought that because some methanol is premixed into the air, the local excess air ratio for diesel is reduced and soot formation is increased. For low diesel fractions, all emission values are dominated by the methanol combustion and soot formation is largely avoided due to the lack of carbon-carbon bonds in the methanol molecule.

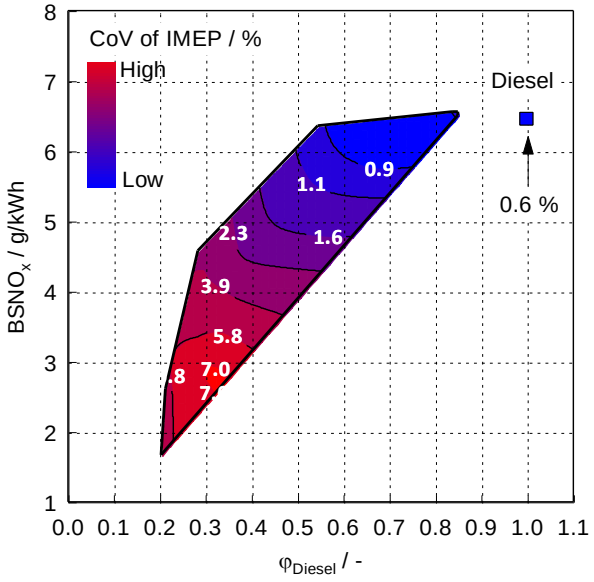

Figure 14. Impact of diesel fraction on combustion stability

The cyclic variability is impacted by the energetic diesel fraction and other factors such as EAR, as shown in Figure 14. A reduced diesel fraction is the strongest indicator of increased cyclic variability due to the higher reliance on flame propagation. Furthermore, at low diesel fractions, the risk for pre-ignitions occurring slightly ahead of the diesel injection increases, which also contributes to an increase in CoV_{IMEP}.

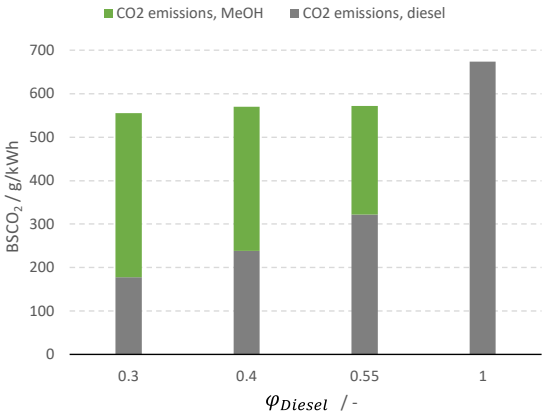

Figure 15. Impact of diesel fraction on CO_2 emissions

The potential for a reduction of greenhouse gas emissions with the introduction of methanol-diesel dual fuel operation is shown in Figure 15 where the brake specific carbon dioxide emissions from the combustion process with EAR = 2.3 are displayed for different diesel fractions (CO_2 emissions from fuel production have not been considered). Total CO_2 emissions decrease with lower diesel fractions due to the lower C/H ratio of methanol, allowing approximately 15 % CO_2 emission reduction with a diesel fraction of 0.3. If methanol is produced from renewable energy sources and with carbon from biogenic sources or direct air capture, the net-CO_2 reduction potential increases to more than 70 % with a diesel energy fraction of 0.3.

6 CONCLUSIONS

Liquid fuels such as methanol have the potential to play a crucial role in the defossilization of hard to abate energy sectors such as transportation if these fuels are produced from renewable sources. To achieve the ambitious GHG reduction targets set by numerous governments and institutions it is necessary to not just focus on newly built vessels and locomotives but to also introduce retrofit options for applications with long service life. Specifically, for retrofit solutions, a diesel-methanol dual fuel combustion concept incorporating a low-pressure methanol injection system might offer a

favorable trade-off between GHG reduction potential and integration effort.

This article presents a multi-stage development process for a diesel-methanol dual fuel concept as a retrofit solution. The process links different methods, including spray characterization, 1D and 3D-CFD simulation as well as SCE testing.

Optical methanol spray investigations in a constant volume spray chamber revealed that for all investigated configurations methanol evaporation was low, indicating that mixture formation in the engine intake port might be challenging. Comparison of the spray angle for selected single-hole spray forming caps showed that with a unity L/D ratio and 50 bar a wider spray angle could be achieved, presumably improving air entrainment and mixture formation. For multi-hole spray forming caps it could be shown that at some point the spray collapse, which has a negative effect on the mixture formation, outweighs the benefit of more and smaller holes and small droplets.

The injection and mixture formation in the locomotive engine was investigated with 3D-CFD simulation. In a first step the model validity for the spray development process was shown via comparison of experimental and simulated spray length and spray cone angle in the spray chamber. In a next step, engine cycle simulations with the validated models were performed. Simulation results suggest that overall smaller droplets lead to a lower wall film mass in the intake manifold, because more droplets are contained in the air flow rather than hitting the walls of the intake manifold. However, it is worth noting that a considerable wall film still forms in the intake manifold because, as observed in the spray chamber test, only a relatively small proportion of the spray evaporates and the majority still contributes to wall film formation. The results further indicate that due to the wall film buildup it is necessary to simulate more than one engine cycle to obtain an (almost) steady-state wall film that evaporates between IVC of the previous cycle and IVO of the current cycle. The fuel vapor is being mixed with air and transported into the cylinder as soon as the intake valves open. The mixing progresses in the cylinder and eventually leads to a homogenous mixture at SOI of the diesel fuel.

Finally, the port fuel injection system with the most promising spray forming caps was tested on the SCE and the influence of the energetic diesel fraction and EAR on combustion performance and exhaust gas emissions was investigated. Operation with an energetic diesel fraction of 0.2 enabled a NO_X emission reduction to 1/3 of the diesel operating point. Emissions of unburned methanol and CO emissions significantly above the levels for diesel operation will likely require exhaust gas aftertreatment. A further reduction of the energetic diesel fraction was limited by high cyclic variability and the occurrence of combustion cycles with pre-ignition. Based on the analysis of simulation and experimental data presented in this paper, the root cause of pre-ignitions at low energetic diesel fraction could not yet be identified. The presence of local fuel-rich mixtures could not be confirmed by 3D-CFD simulations of the mixture formation. Other effects such as wall film detachment that have not been modelled in detail might contribute to local fuel rich zones. Other potential root causes might include burning oil droplets or hot surfaces which act as an ignition source. In order to investigate this phenomenon and identify key impact parameters in detail, additional measurements on the SCE are needed.

7 DEFINITIONS, ACRONYMS, ABBREVIATIONS

AFR: Stoichiometric air/fuel ratio of diesel fuel

BSCO: Brake specific carbon monoxide emissions

BSNO$_X$: Brake specific nitrogen oxides emissions

BSMeOH: Brake specific methanol emissions

CA: Crank angle

CFD: Computational fluid dynamics

COV$_{IMEP}$: Coefficient of variation of IMEP

CO$_2$: Carbon dioxide

DBI: Diffused back illumination

DDM: Discrete droplet method

DoC: Duration of current

EAR: excess air ratio

EAR$_{gl}$: Global excess air ratio

EAR$_{meth}$: Methanol excess air ratio

FRA: Federal railroad administration

GHG: Greenhouse gas

GWP: Global warming potential

HRR: Heat release rate

IMEP: Indicated mean effective pressure

IVO: Intake valve opening

IVC: Intake valve closing

L/D: length to diameter ratio

MCE: Multi-cylinder engine

MFB50%: Mass fraction burned 50 %

N: Engine speed

NO_X: Nitrogen oxides

N_2: Nitrogen

PFI: Port fuel injection

RANS: Reynolds averaged navier stokes

ROI: rate of injection

SCE: Single cylinder research engine

SOI: Start of injection

SMD: Sauter mean diameter

SOI: Start of injection

TDC: Top dead center

UI: Uniformity index

8 ACKNOWLEDGMENTS

The authors would like to acknowledge the financial support of the "COMET - Competence Centers for Excellent Technologies" Program of the Austrian Federal Ministry for Climate Action, Environment, Energy, Mobility, Innovation and Technology (BMK) and the Austrian Federal Ministry of Labor and Economy (BMAW) and the Provinces of Salzburg, Styria and Tyrol for the COMET Centre (K1) LEC GETS. The COMET Program is managed by the Austrian Research Promotion Agency (FFG). The author would also like to thank Angelika Sauer-Malin for her great input to this paper.

9 REFERENCES AND BIBLIOGRAPHY

[1] Copernicus Climate Change Service. 2024. 2024 virtually certain to be the warmest year and first year above 1.5°C, https://climate.copernicus.eu/copernicus-2024-virtually-certain-be-warmest-year-and-first-year-above-15degc (accessed on January 3, 2025).

[2] EPA. 2024. Sources of greenhouse gas emissions, https://www.epa.gov/ghgemissions/sources-greenhouse-gas-emissions (accessed on January 3, 2025).

[3] Federal Railroad Administration. 2025. FRA's Climate and Sustainability Program, https://railroads.dot.gov/rail-network-development/environment/fras-climate-and-sustainability-program (accessed on January 3, 2025).

[4] Union Pacific. 2023. What Are Railroads Doing About Climate Change?, https://www.up.com/customers/track-record/tr040423-how-railroads-address-climate-change-2023.htm (accessed on January 3, 2025).

[5] Vale. Decarbonization strategy and management, https://vale.com/esg/decarbonization-strategy-and-management (accessed on January 3, 2025).

[6] EIT Urban Mobility. Iarnród Éireann Irish Rail & DIGAS team up to retrofit Europe's first hydrogen-powered freight locomotive, https://www.eiturbanmobility.eu/iarnrod-eireann-irish-rail-digas-team-up-to-retrofit-europes-first-hydrogen-powered-freight-locomotive/ (accessed on January 3, 2025).

[7] EU Commission. Reducing emissions from the shipping sector, https://climate.ec.europa.eu/eu-action/transport/reducing-emissions-shipping-sector_en (accessed on January 3, 2025)

[8] European Union. 2023. Regulation (EU) 2023/1805 of the European Parliament and of the Council of 13 September 2023 on the use of renewable and low-carbon fuels in maritime transport, and amending Directive 2009/16/EC, https://eur-lex.europa.eu/legal-content/EN/TXT/?uri=CELEX%3A32023R1805 (accessed on January 3, 2025).

[9] The United States Government. 2024. An Action Plan for Maritime Energy and Emissions Innovation, https://www.energy.gov/sites/default/files/2024-12/doe-eere-modal-reports_maritime-energy-emissions-innovation-action-plan.pdf (accessed on January 3, 2025).

[10] Veracity by DNV. Alternative Fuels Insight, https://store.veracity.com/premium-access-alternative-fuels-insight-afi?utm_campaign=ma_glob_afi_alltime#_gl=1*1ez9t09*_gcl_au*MjA5OTI2MzkyOC4xNzM1Mzk5MDg1 (accessed on January 3, 2025).

[11] LR. 2023. Engine retrofit report 2023, https://maritime.lr.org/l/941163/2023-10-04/8g57x/941163/16964222981dLpRlSP/LR_101507_P4_Engine_Retrofit_Guide_v8.pdf (accessed on January 3, 2025).

[12] International Maritime Organization. 2020. Interim guidelines for the safety of ships using methyl / ethyl alcohol as fuel, https://www.register-iri.com/wp-content/uploads/MSC.1-Circ.1621.pdf (accessed on January 3, 2025).

[13] Repo, J. 2023. Methanol combustion concept alternatives for new build and retrofit of 4-stroke medium speed engines, CIMAC Congress 2023, Busan, South Korea.

[14] Mattheeuws, L., 2019, ABC's Dual-fuel engines running on renewable fuels like methanol and hydrogen. *CIMAC Congress 2019*, Vancouver, Canada.

[15] Kunkel, C., Hagl, P., Manickam, B., Gross, C. Eppler, F. 2024. Methanol retrofits for a fast net-CO2 reduction in the marine market. *13. Dessauer Gasmotoren-Konferenz*, Dessau, Germany.

[16] AVL List GmbH. 2024. *Spray module, AVL FIRE™ M User Manual*, Version R2023.2.

[17] Sorrentino, A. 2023. Methanol port fuel injection for medium-speed application: injector development and engine design. *CIMAC Congress 2023*, Busan, South Korea.

[18] Hiroyasu, H. and Arai, M. 1990. Structures of Fuel Sprays in Diesel Engines. SAE Technical Paper 900475.

[19] AVL List GmbH. 2023. uniformity_index.frml, AVL FIRE™ M Version 2023.2, cfdIntegrate formulae.

[20] Dodge, L. and Naegeli, D. 1994. Injector Spray Characterization of Methanol in Reciprocating Engines, *NREL/TP-425-6344*, National Renewable Energy Laboratory.

[21] Möhwald Einspritzsysteme. 2025. Einspritzanalysator HDA, https://www.boschmanufacturingsolutions.com/de/produkte-und-services/processes/messen-und-pruefen/pruefsysteme/testing-technology-injectionsystems-live.html (accessed on January 10, 2025).

[22] Manin, J., Bardi, M., Pickett, L. 2012. Evaluation of the liquid length via diffused back-illumination imaging in vaporizing diesel sprays, the eighth International conference on modelling and diagnostics for advanced engine systems (COMODIA 2012), Japan.

[23] Settles, G. 2001. Schlieren and Shadowgraph Techniques: Visualizing Phenomena in Transparent Media, 1st edition, Berlin Heidelberg New York, pp. 25 ff.

[24] Malin, M., Krivopolianskii, V., Rygh, B. et al. 2015. Soot Investigation on Fish Oil Spray Combustion in a Constant Volume Cell, SAE Technical Paper, 2015-24-2479.

[25] Pickett, L. M. 2018. Liquid extinction analysis compared to CFD, ECN Workshop ECN6, https://ecn.sandia.gov/G/data/liq/LiquidPickett Mar2018.pptx (accessed on January 16 2025).

[26] Stahl, M. 2008. Experimentelle und numerische Untersuchung des primären Strahlzerfalls von Druckzerstäubern, Dissertation, Fachbereich Maschinenbau, Technischen Universität Darmstadt, pp. 4-15.

[27] Wei, Y., Li, T., Zhou, X., et al. 2020. Time-resolved measurement of the near-nozzle air entrainment of high-pressure diesel spray by high-speed micro-PTV technique, Fuel, 268(117343).

[28] Ainsalo, A., Sallinen, R., Kaario. O. et al. 2019. Optical investigation of Spray characteristics for light fuel oil, kerosene, hexane, methanol and Propane, Atomization and Sprays, 29(6):521–544.

[29] Varde, K.; Popa, D.; Varde, L. 1984. Spray Angle and Atomization in Diesel Sprays, SAE Transactions, Vol. 93, 840772–841109, pp. 779-787.

[30] Oh, H.; Hwang.; White, L. et al. 2022. Spray collapse characteristics of practical GDI spray for lateral-mounted GDI engines, International Journal of Heat and Mass Transfer, 190 (2022) 122743.

[31] Verhelst, S., Turner, J., Sileghem, L., et al. 2019. Methanol as a fuel for internal combustion engines, Progress in Energy and Combustion Science, 70 (2019) 43–88.

[32] Weiss, L., Wensing, M., Hwang, J., et al. 2020. Development of limited-view tomography for measurement of Spray G plume direction and liquid volume fraction, *Experiments in Fluids,* 61(51).

[33] Payri, F., Payri, R., Bardi, M., et al. 2014. Engine combustion network: Influence of the gas properties on the spray penetration and spreading angle, *Experimental Thermal and Fluid Science*, 53: 236-243.

10 CONTACT

Dipl.-Ing. Dr.techn. Maximilian Malin
Tel.: +43 316 873-30093
Fax: +43 316 873-30102
Inffeldgasse 19, 8010 Graz, Austria
Email: maximililan.malin@lec.tugraz.at